PAPER

Fire ant rafts elongate under fluid flows

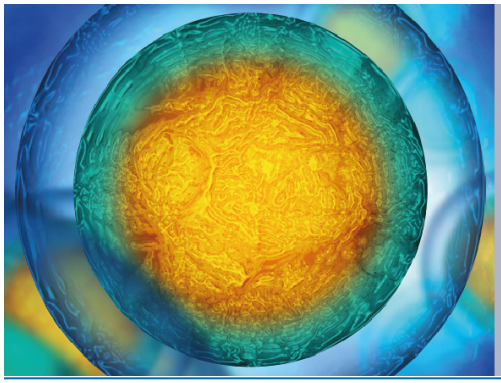

Bioinspiration & Biomimetics

PAPER

Fire ant rafts elongate under fluid flows

Hungtang Ko[1], Ting-Ying Yu[2] and David L Hu[1,3,*]

[1] George W. Woodruff School of Mechanical Engineering, Georgia Institute of Technology, United States of America
[2] School of Electrical and Computer Engineering, Georgia Institute of Technology, United States of America
[3] School of Biology, Georgia Institute of Technology, United States of America
[*] Author to whom any correspondence should be addressed.

E-mail: hu@me.gatech.edu

RECEIVED
14 December 2021

REVISED
5 May 2022

ACCEPTED FOR PUBLICATION
6 May 2022

PUBLISHED
9 June 2022

Keywords: collective behavior, fluid-structure interaction, drag reduction, fire ant rafts

Supplementary material for this article is available online

Abstract

Fire ants survive flash floods by linking their bodies together to build waterproof rafts. Most studies of fire ant rafts consider static water conditions, but here, we consider the influence of flow. In particular, when floating on shallow water, the raft can run aground on vegetation, generating stresses in the raft as the water continues to flow around it. In this combined experimental and numerical study, we film the 10 h response of a fire ant raft caught on an anchor and subjected to water flows of 6 cm s^{-1}. In this situation, ant rafts elongate from circular to more streamlined shapes, doubling in aspect ratio before eventually contracting back into smaller circular shapes as they enter dormancy. Ants in upstream regions of the raft exhibit less exploration activity than those downstream, suggesting that ants migrate to areas of lower fluid stress. While the raft is rough, hydrophobic, and heterogeneous in height, we may gain some insight by performing both fluid-structure interaction and agent based simulations on smooth rafts. Elongation to the degree observed is associated with a 48% drag reduction. Moreover, a purely elastic raft does not elongate, but conversely increases its bluff body cross-sectional area. We conclude that ant raftsmust reconfigure to generate the elongated shape observed. This work may provide insights into designing intelligent robotic swarms that can adapt to fluid flows.

1. Introduction

Fire ants *Solenopsis invicta* build rafts composed of up to 100 000 individuals in order to survive seasonal flooding in their native habitat, the Pantanal wetlands of Brazil [1, 2]. The ant raft often drifts in shallow waters, which creates many opportunities for it to run aground on sticks, logs, and other protruding vegetation, as shown in figure 1(A). Such conditions apply stresses to the raft due to the anchorage point and surrounding flow pulling the raft in opposite directions. How can the raft resist being torn apart, especially since each individual ant can only sense their local environment? In this paper, we perform experiments and a simplified numerical analysis to unravel this complex process.

Most studies of animal aggregations assume static fluid conditions., but in reality, winds and rivers flow. Carrying out such controlled situations in the laboratory is difficult. One scenario that has been studied is the collective behavior of a few fish in a water tunnel. In comparison, fire ants are an ideal swarm to study because their aggregations are generally two-dimensional, and their small body size allows them to be studied easily in greater numbers. In nature, fire ant rafts can be buffeted by many dynamic forces on the water surface, including capillary waves, and the turbulence associated with water flowing over rocks. Nevertheless, most previous work on fire ant rafts has been done on static water surfaces [1, 3, 4].

Outside the world of animal swarms, other biological materials have been shown to reconfigure under fluid flows. In fact, reconfiguration is essential for the survival of organisms in fluid habitats whose natural state is turbulent and unstable [5]. Marine plants such as seaweed, sea pens, and giant reeds adopt flow-dependent shapes to cope with fast water currents [6–9]. Flexibility also allows soft corals (gorgonians) to reduce drag [10–12]. On land, plants interact with the wind across a variety of length scales, from the

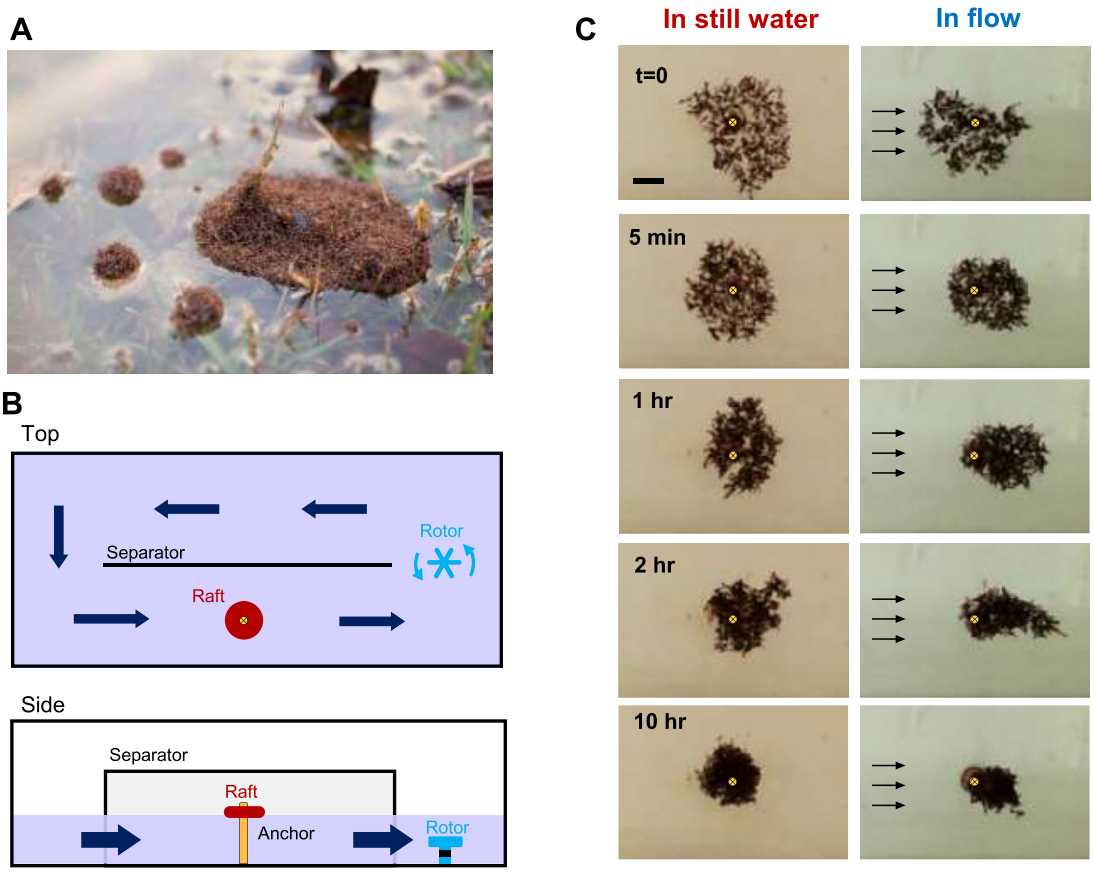

Figure 1. (A) Natural fire ant rafts (photo from Shutterstock.com). (B) Schematic of the water tunnel. (C) Time course of the ant raft in still water (left) and in flow (right). The yellow cross symbols present the anchorage point.

swaying of trees trunks to the deformation of leaves [13–15]. Vogel showed that broad leaves reconfigure and reduce aerodynamic drag in high winds [16]. Tree crowns also streamline with the wind, which decreases their drag coefficient with increasing wind velocity [17–19]. The mechanical response of plants can be more than just fleeting: in regions with strong and persistent winds, plants may deform permanently [15, 20, 21]. For plants, such deformation typically takes days or weeks. Studying fire ants allow us to observe shape deformation on faster time scales. Moreover, since the individuals of an ant raft are millimeters in scale, it is easier to track their movement than the cells of growing structures like plants.

Animal aggregations respond to disturbances in ways that passive materials cannot. For example, aggregates of live ants can flow like a fluid, whereas dead ants act only as a granular solid [22]. Tennenbaum *et al* measured the viscoelasticity of live and dead fire ant aggregates using shear rheometry. They found that live ant aggregates have lower elastic and viscous moduli than dead ants due to their ability to rearrange, making them more fluid-like and flexible [22]. Similarly, live black soldier fly larva aggregates relax under applied forces faster than dead larvae [23]. Swarming midges display viscoelastic properties with a high viscous modulus [24]. If their substrate oscillates, honeybee swarms actively flatten to reduce stress [25]. This body of work shows that the language of rheology, which typically describes the flow and deformation of inanimate materials, can be used to describe the response of living materials to their surroundings. However, these previous studies are still somewhat unnatural as they only consider using the displacement of solid boundaries as perturbations. In this study, we examine how fluid flow perturbs the shape of ant rafts.

2. Materials and methods

2.1. Water tunnel experiments

We collected fire ants from the campus of the Georgia Institute of Technology in Atlanta, Georgia. Experiments were conducted within two months of collection, and ants were fed water, honey jelly, dried crickets, and fly larvae. In each trial, we manually picked out 0.25 g (around 250 individuals) of ant workers. All rafts were created by first placing the ants into a beaker coated with insect-a-slip (Fluon) and swirling the beaker to form a dense ball of ants [1]. After an ant ball was made, we immediately transferred it to the top of a 10.5 cm-long bolt, which served as the anchor for the raft.

A low-speed water tunnel was built using a ten-gallon aquarium (26 × 30 × 50 cm). Flow was

generated with a magnetic rotor salvaged from an underwater pump (Marineland Maxi-Jet) and actuated by a hot plate stirrer (Corning PC-220). A schematic of the water tunnel is shown in figure 1(B). The experiments were conducted in a 13 cm wide channel with a 6 cm s^{-1} uniform flow. The flow speed and uniformity were confirmed by tracking floating Styrofoam balls (around 5 mm in diameter). Using our current setup, doubling the flow rate created significant waves at the water surface. Thus, only one flow speed was recorded with the ants. We recorded the top view of the rafts using an HD webcam (Aoni C33) placed 17 cm above the water surface. Due to the meniscus at the aquarium wall, we could not capture the side view of the rafts. A time-lapse video was recorded, with one snapshot taken every 10 s for 10 h, using a custom code in MATLAB. Therefore, we collected 3600 snapshots for each trial.

In our study, we filmed four successful trials of 250 ants in water flows of 6 cm s^{-1} for 10 h. We tried varying aspects of this test, including the number of ants, the flow speed, and the duration, but by process of trial and error, we found that the only repeatable test was the regime presented. We briefly discuss the challenges associated with varying these parameters, beginning with the flow speed.

We did not decrease the flow speed because the response will be less significant, decreasing the signal-to-noise ratio. Deformation might require experiments longer than 10 h. We built a larger experimental apparatus to accommodate higher a flow speed of 15 cm s^{-1}. However, these experiments resulted in several difficulties. Increasing flow speed creates a number of unsteady disturbances, such as turbulent flow and capillary waves. Steady capillary waves occur at the capillary wave speed of 23 cm s^{-1}, but transient waves are generated from slower speeds. Consequently, the raft was often torn apart or separated from the anchor before it had a chance to deform adequately. Moreover, visualization of the ant raft shape requires a smooth water surface, which is impeded by turbulence.

Increasing raft sizes introduces similar challenges with lower flow speeds, i.e. less significant responses over longer time scales. Our rafts are already small. Reducing the size further requires an even smaller anchor, and the deformation will be less evident because fewer ants are available to perform the task. Studying ant raft deformation on the water surface is indeed a balance of experimental design and the fragile nature of ant network.

2.2. The anchor

In nature, ant rafts can anchor onto a range of surfaces, from floating logs to protruding vegetation of various surface properties and shapes. Since our goal is to model the deformation of the raft, we created an anchor that would have a minimal influence on the raft. Our anchor consisted of a submerged bolt protruding from the water surface by approximately 0.1 cm. We found that this protrusion amount was tall enough that the ants could grip onto it with their sticky feet, but not so tall that they could build a tower above the water surface and thus avoid fluid flows. There is a small range of flow speed that can be used in this experiment because the flow speed must be high enough to deform the raft but not to break the ants' grip on the anchor.

2.3. Image and data processing

Video analysis was performed in MATLAB. We first cropped and binarized the images, then extracted metrics of interest using the 'regionprops' function within the image processing toolbox. We measured the raft area, perimeter, and centroid location. Upon fitting the rafts to ellipses, we measured the lengths of the major and minor axis and the orientation with respect to flow.

Our system is characterized by the following dimensionless groups, which include the Reynolds number Re, drag coefficient C_D, raft dimensionless length L^*, thickness T^*, displacement x^*, and angle ϕ:

$$\mathrm{Re} = \frac{\rho U W}{\mu}, \tag{1}$$

$$C_D = \frac{2F_D}{\rho U^2 W T}, \tag{2}$$

$$L^* = L/W, \tag{3}$$

$$T^* = T/L, \tag{4}$$

$$x^* = x/L, \tag{5}$$

$$\phi \tag{6}$$

where ρ and μ are the density and dynamic viscosity of water, U is the uniform flow velocity, and F_D is the fluid drag. As shown by the schematic in figure 2(A), a raft can shift in angle ϕ due to rotation around the anchor point. The raft's longest axis is characterized by a length L, and the remaining dimensions by width W and thickness T. The dimensionless length L^* is the raft's length L normalized by its width W; similarly, the dimensionless thickness T^* is the raft's thickness normalized by its width W. As the raft deforms in the flow, its centroid displaces a distance x relative to the raft's anchorage point (yellow crosses in figure 2(A)), which remains fixed to the lab frame. The dimensionless displacement x^* is defined as the displacement x divided by the raft length L.

To quantify ant activity at the edge of the raft, we first extracted the perimeter of the rafts by transforming camera images into binary based on a fixed gray-scale threshold. Raft perimeters in the binary images may be written in Cartesian coordinates $[x(s,t), y(s,t)]$, parameterized in terms of arc length s and time t. We transformed the perimeters into polar coordinates $[r(s,t), \theta(s,t)]$. Since the rafts were generally convex, we neglected the dependence on arc length and wrote the perimeter $r(\theta, t)$ as a function

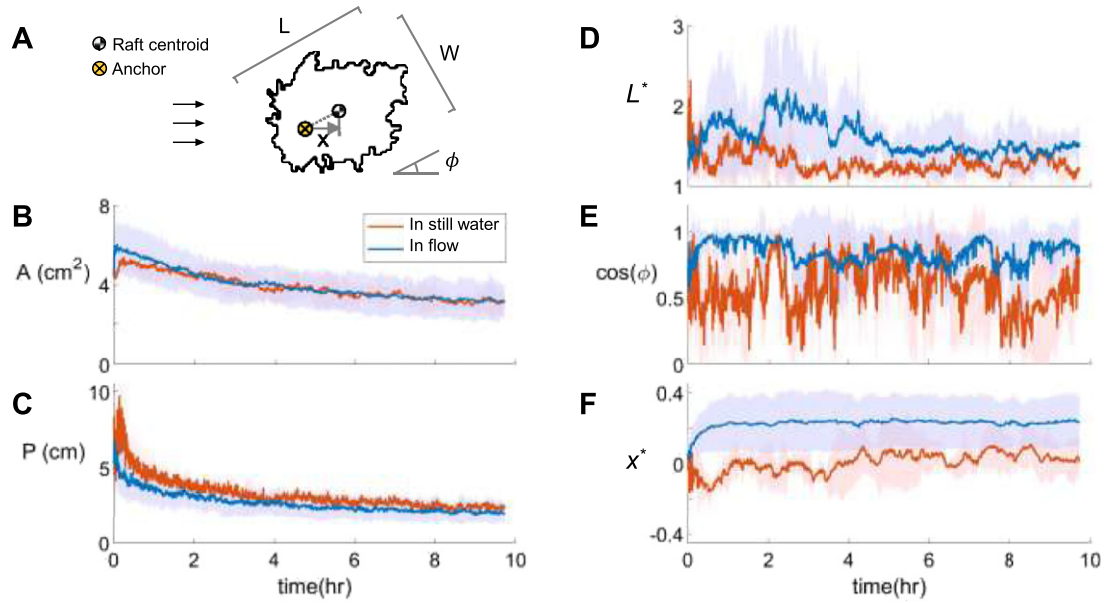

Figure 2. Raft deformation dynamics. (A) A schematic of the raft with variables for geometry and orientation. Time series for (B) raft area, (C) raft perimeter , (D) raft dimensionless length L^*, (E) cosine of raft orientation ϕ, and (F) dimensionless displacement of the raft x^*. Red and blue represent experiments in still water and in flow, respectively. The height of the shaded region is twice the standard deviation.

of θ and t alone. Then, we calculated the absolute difference of the radius for two consecutive raft shapes at a fixed time interval Δt apart:

$$\Delta r(\theta, t) = |r(\theta, t + \Delta t) - r(\theta, t)|. \quad (7)$$

Our camera recorded a frame every $\Delta t = 10$ s. As ants approached and departed the raft boundary, we observed $\Delta r(\theta, t)$ on the order of 1 mm, which is comparable to the ant body length of 3 mm. We thus used $\Delta r(\theta, t)$ as a proxy for boundary exploration activity.

We measured the contraction rate of the raft using optical flow. The displacement field between two snapshots was obtained with the Horn–Schunck method [26]. We then calculated the average of the displacement field over durations of 2.5 h.

2.4. Computational fluid simulations

To estimate the drag coefficient and streamlines around a smooth two-dimensional ant raft, we performed 3D simulations using COMSOL Multiphysics. The fluid and solid fields were fully coupled on the raft's deformable boundary. The fluid was assigned the properties of water, including density, viscosity, and incompressibility. We assumed a purely elastic raft characterized by the linear elastic modulus $E = 200$ Pa and Poisson ratio $\nu = 0.3$, measured on a fire ant aggregation using a rheometer [22]. We acknowledge ant aggregations display viscoelastic properties due to their active rearrangement [22]. However, our results using a purely elastic raft are identical to the equilibrium shapes of viscoelastic rafts composed of Kelvin–Voigt materials.

In the simulation, the water tunnel was 100 cm long, 15 cm wide, and 15 cm deep in order to reduce edge effects. The anchor for the raft was a cylinder of 0.25 cm in diameter and 15 cm in height. We tested a range of raft elliptical aspect ratios, all having a plan view area of π cm^2 (or effective radius of 1 cm) and 1 cm in raft thickness. These values are comparable to our experiments in which the ant raft began at 4 cm^2 in area. We did not measure the raft thickness, but previous work [1] suggests ant rafts have an average thickness of 3.75 mm.

To ensure the stability of the computation, we initiated the simulation with a water flow ramping up from 0 to 6 cm s^{-1} across a duration of $t = 12$ s. The flow quickly stabilized after the plateau, with no oscillatory patterns. We continued the simulation for $t = 60$ s and recorded the equilibrium solution at the last time step. We performed parameter studies varying the initial dimensionless length L^* from 1 to 2, and dimensionless displacement x^* from -0.4 to 0.4.

2.5. Agent-based simulations

As we saw in our simulations, he relative movement of ants in the raft could not be captured using a solid continuum model. Therefore, we turned to agent-based simulations. This approach came at the cost of lower fidelity than the computational fluid dynamic simulations. We assumed a static flow field, namely the potential flow generated around the cylindircal anchor. The anchor was assumed to have twice the size of an agent, matching the relative size of the anchor in the experiment. We performed two-dimensional simulations consisted of one stationary agent representing the anchor and 30 circular agents that move

according to Newton's 2nd law. There were five external forces:

- Fluid force $\vec{F}_{\text{fluid}}$. A force proportional to the local flow velocity vector. From the potential flow theory [27], we used $\vec{F}_{\text{fluid}} = f_{\text{fluid}}[1 + 4\frac{y^2-x^2}{(x^2+y^2)^2}, -8\frac{xy}{(x^2+y^2)^2}]$, where x and y are the coordinates of the ant.
- Inward attraction $\vec{F}_{\text{anchor}}$. A constant attraction towards the anchor.
- Cohesion $\vec{F}_{\text{cohesion}}$. A constant attraction between neighboring ants.
- Repulsion $\vec{F}_{\text{repulsion}} = k_{\text{repulsion}}d$. A force proportional to inter-agent distance d, pointing away from the neighbor. $\vec{F}_{\text{repulsion}}$ was applied only when two agents overlap.
- Damping $\vec{F}_{\text{damping}} = -k_{\text{damping}}\vec{u}$. A virtual damping force proportional to the agent's velocity $\vec{u}$. This mechanism does not affect the results significantly but helps stabilize the simulation.

The simulation was carried out in dimensionless parameters, scaled with the radius and mass of the particle. The time scale of the simulations can be interpreted arbitrarily. In the simulations, we used time steps $\Delta t = 0.1$, $k_{\text{fluid}} = 0$ to 11, $F_{\text{anchor}} = 10$, $F_{\text{cohesion}} = 0.5$, and $k_{\text{damping}} = 10$. We used the ratio between the fluid force and the attraction towards the anchor, $F = f_{\text{fluid}}/F_{\text{attraction}}$, as a proxy for flow intensity.

3. Results

3.1. Streamlining under uniform flow

Our water speed is slower than natural rivers such as the Sacramento River and its tributaries, Sutter Slough, which have surface speeds of 40 cm s^{-1} far from shore [28]. At 50 cm away from the river bank, the flow velocity decreases to around 10 cm s^{-1}. Fire ants evolved in the Pantanal wetlands, which flow slower than rivers. Stern *et al* measured the velocity of a natural wetland in located Westchester, NY, to be around 8 cm s^{-1} [29], which is comparable to the speed in our experiments. Based on the raft's initial width $W \approx 2$ cm, the Reynolds number in our expeirments $\text{Re}_W = 1200$.

We focus our analysis on the plane view of the raft. Figure 1(C) and the supplemental video (https://stacks.iop.org/BB/17/045007/mmedia) show a pair of time series of raft shapes for still water (left) and flow (right). For the raft in flow, the water travels to the right, as shown by the arrows. The yellow cross designates the anchor. Previous work showed that an ant ball expands rapidly into a raft within minutes of being placed on the water surface [1]. We confirm this initial growth, as demonstrated by the time course of the raft area shown in figure 2(B). Rafts in both conditions begin with a surface of 4 cm^2. Rafts in flow grow to a surface area of 6 cm^2 (blue line in figure 2(B)), while rafts in still water only grow to an average surface area of 5 cm^2 (red line in figure 2(B)). The shaded blue and red regions show the standard deviations for the rafts in flow and in still water, respectively. During the rapid expansion period, ants walk frantically away from the center of the raft and move towards the edges [1]. Since the raft in flow expands to a larger amount, it appears that the flow accentuates this outward migration.

The rapid expansion of the raft to an area A of 5–6 cm^2 is followed by a slow, nearly linear contraction to an area of 3 cm^2 on the scale of hours. At the end of 10 h, the raft was still shrinking, and had not reached equilibrium. The time course of the area A and perimeter P of the raft is shown in figures 2(B) and (C). The contraction rate of area and perimeter is comparable for both conditions. However, rafts in still water have rougher boundaries, leading to slightly longer perimeters (figure 1(B)).

Figure 2(D) shows the time course of the dimensionless raft length. For rafts in flow, the dimensionless lengthL^* grows to as large as 2–3 as the raft elongates downstream over 3–4 h. In comparison, the raft in still water only expands to a dimensionless length of 1.5. Afterwards, both rafts shrink, reducing in L^* after 5 h.

Figure 2(E) shows the time course of the cosine of the angle of the raft. Here, $\cos(\phi) \approx 1$ is associated with $\phi \approx 0$, indicating the alignment of the raft with the flow direction. Rafts in flow align their long axis with the flow direction, while rafts in still water are randomly orientated. In any case, asymmetry is a signature of both rafts in flow and in still water. Many structures built by ants such as towers, rafts, and the mounds built by termites are asymmetric. The ants in still water can be drawn by fluctuating environmental conditions such as light, shadows, and temperature. Evidently, these effects are dominated by the influence of flow .

Figure 2(F) shows the time course of the raft displacement, the distance the center of mass travels from the anchorage point. In flow, the dimensionless displacement $x^* \approx 0.25$, meaning that the raft centroid displaces a quarter of the raft length downstream from the anchor. As expected, in still water, $x^* \approx 0$, indicating that the center of the raft remains near its original position at the anchor. Thus, although rafts in both conditions were elliptical, only the raft in flow displaced its center of mass. Even in still water, rafts constantly deform, as shown by the fluctuations in displacement in figure 2(F). Fluctuations in raft displacement and raft shape are associated with ants on the surface exploring the raft boundary. Since the ants have only local visual and tactile sensing, only by approaching the edge can they obtain information about

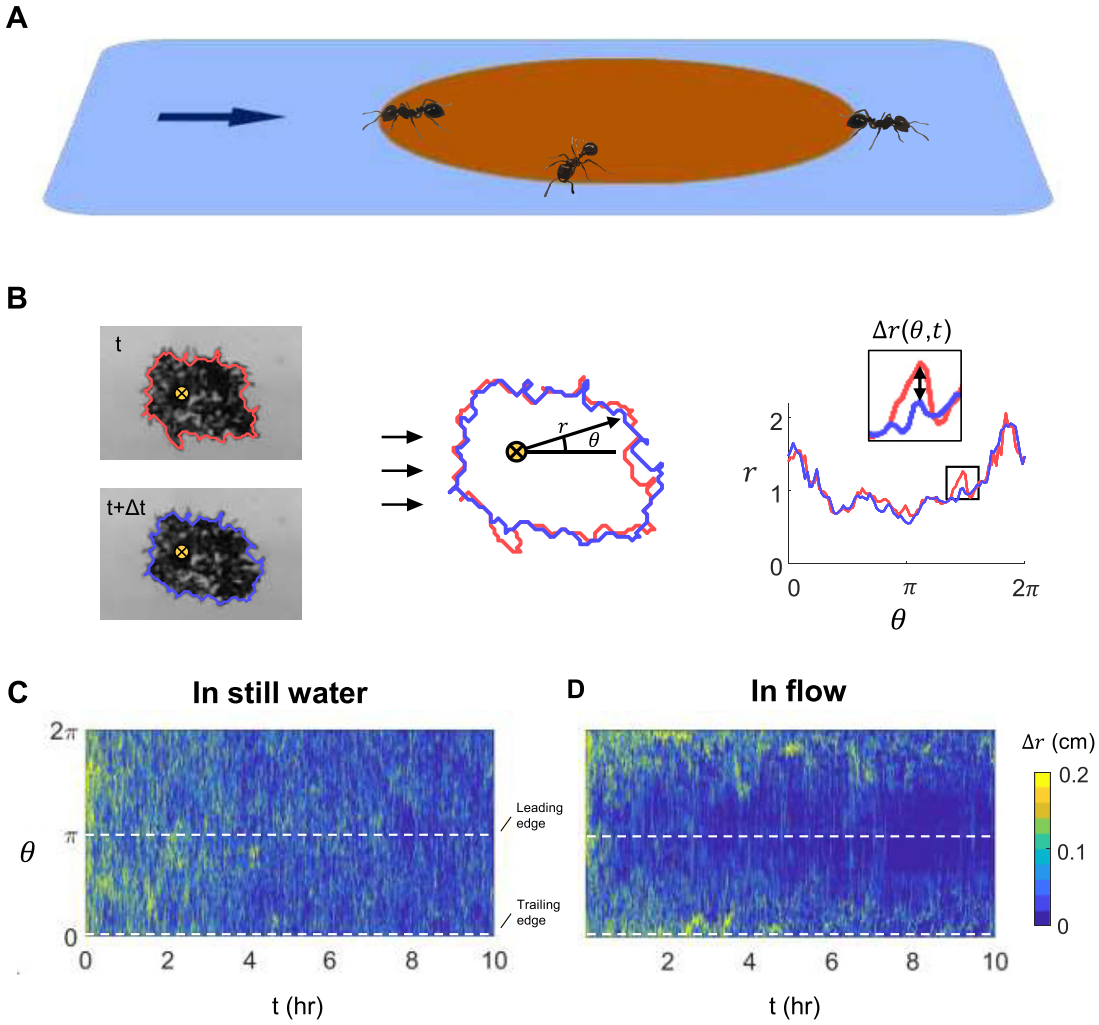

Figure 3. The activity of ants at the raft's perimeter . (A) Schematic showing ants exploring the boundary of a raft. The blue arrow indicates the direction of water flow. (B) Steps for calculating the ant activity level $\Delta r(\theta, t)$, the difference in radii of the rafts at two points in time. The sample graph on the right shows the relationship between $\Delta r(\theta)$ and angle θ for a single instant in time. Heat maps of $\Delta r(\theta, t)$ for rafts (C) in still water and (D) in flow. The dotted lines mark the leading and trailing edge of the raft.

the flow. In the next section, we present how such activity vary with ants' location relative to the raft.

3.2. Activity level and contraction rate

We begin by introducing the basic structure of the raft. Previous work has shown that an ant raft is composed of two layers [1]. The bottom layer is a structural layer of stationary ants; the top layer is free-roaming. The shape of the raft is determined by two opposing mechanisms. On the one hand, free-roaming ants on the top explore and occasionally settle down at the boundary of the raft to expand it. On a slower time scale, ants in the structural layer occasionally leave their positions, causing the raft to contract slowly. At equilibrium, these two mechanisms balance, resulting in a raft that does not change in shape or size. As we show in figure 2(B), at the beginning stages of raft construction, exploration activity outweighs contraction, causing rafts to expand. Then, the balance is reversed and rafts start to shrink slowly over a few hours. In this section, we track both the contraction and the exploration behaviors with image analysis.

In equation (7) in the materials and methods section, we define a proxy for local activity level as $\Delta r(\theta, t)$, with large Δr indicating large radial contractions or expansions over that time interval, and $\Delta r = 0$ indicating no change. The schematic in figure 3(B) shows how the $\Delta r(\theta, t)$ of the raft is defined. Figures 3(C) and (D) shows the heat maps of ant activity Δr for ant rafts in still water (left) and in flow (right). The activity level Δr is shown as a function of azimuthal position θ around the raft and time t, with the color showing activity level (yellow being the most active).

In both still water and flow, the activity level is highest in the first 2 h as the ants get acclimated to being placed on water. In this phase, ants in flow appear to be more subdued, as shown by the lower amount of yellow color in the graph. After the initial phase, ant activity in still water is homogeneous, with $\Delta r(\theta, t)$ being uniform at different values of θ. In stark

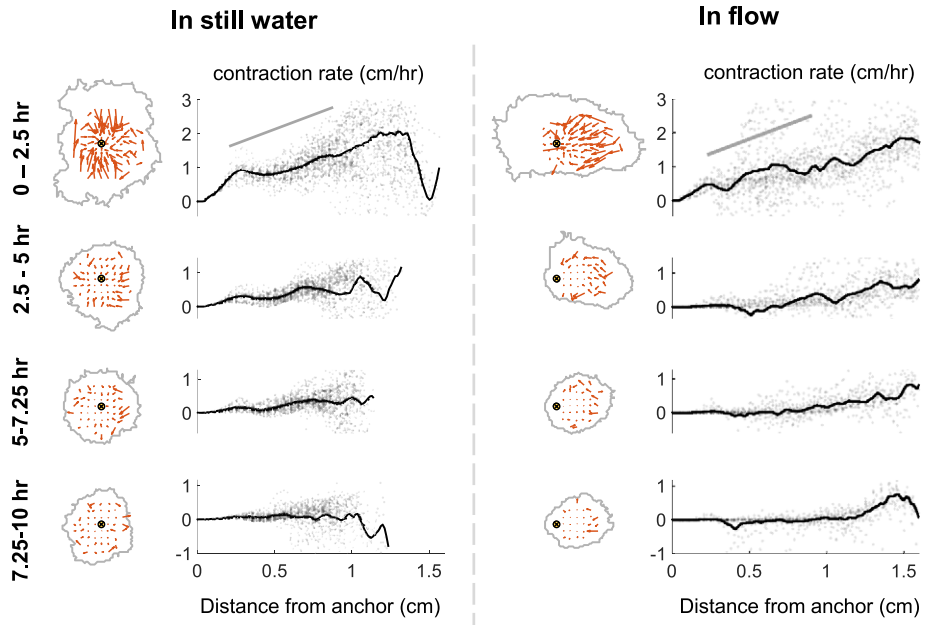

Figure 4. Contraction of the fire ant raft in still water (left) and in flow (right). Four time windows are shown across the 10 h trial. Orange arrows show the instantaneous velocity of points on the raft. Graphs show the relationship between contraction velocity and radial distance from the anchor. The dots represent the data at different locations and time instants, and the solid lines represent the average.

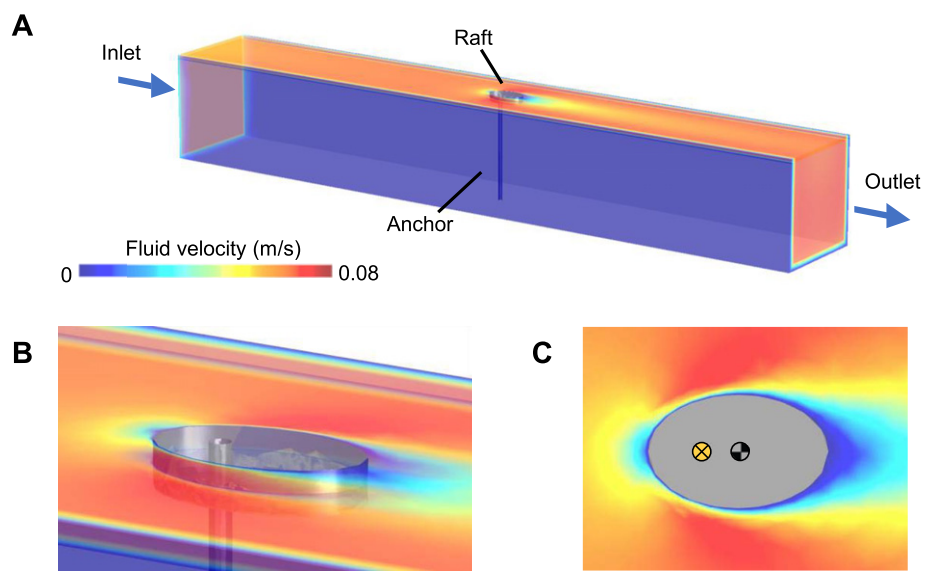

Figure 5. Fluid-structure interaction simulations of an elastic raft in flow. (A) Domain of the simulation includes a water inlet, outlet, a raft, and a bolt that anchors the raft. Color shows the fluid velocity. An oblique (B) and overhead (C) view of the flow field around the raft. Yellow crosses indicate anchorage point and the circle with shaded quadrants indicates center of mass.

contrast, rafts in flow have the highest activity is in the downstream direction, marked by $\theta = 0$ and $\theta = 2\pi$. The flow clearly introducesa directional bias in the exploration activity of the ants. Indeed, as shown in the schematic (figure 3(A)), we observe that ants at the leading edge often only use antennae to explore the water. In contrast, ants at the trailing edge walke their entire bodies onto the water surface to explore.

The streamlining process of ant rafts is a consequence of active migration, not fluid erosion. In erosion, fluid stresses exceed the fracture strength of the material, causing particles to dislodge. Two ants [1] can support up to 620 dynes (6.2 mN) in tension, which is similar to the weight of the entire raft (2.5 mN). It is unlikely that such a slow flow can break the connections between pairs of ants. Instead, the fluid stresses gently guide the ant's exploration.

The process by which ants migrate from stationary locations remains unknown, but it is likely due to multiple interactions between the ants and flowing water. We originally tracked the sign of $r(\theta, t)$ to determine when ants would leave a stationary spot

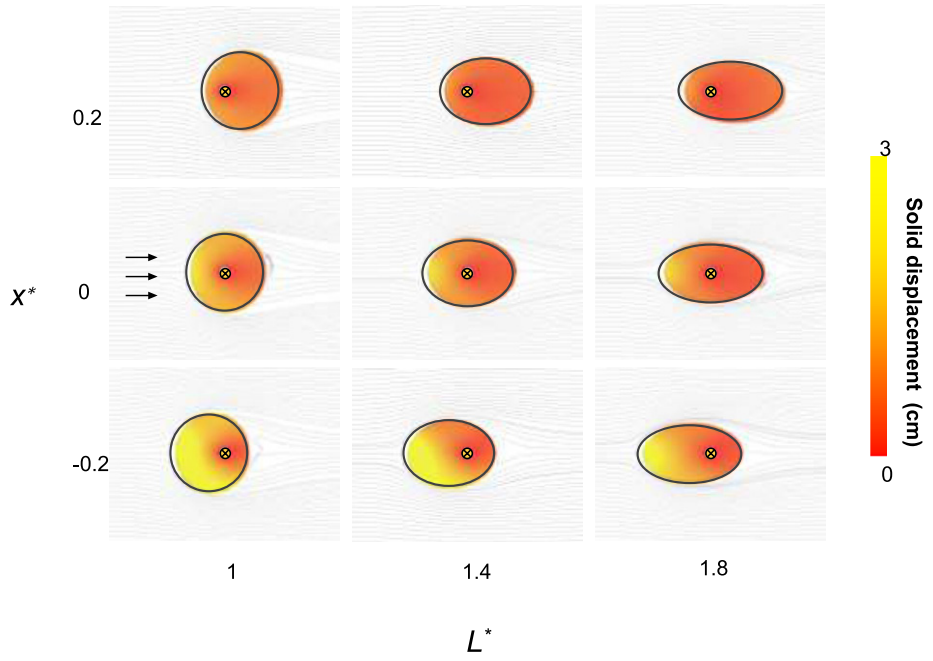

Figure 6. Simulation results for deformation of an elastic raft. On the horizontal axis, dimensionless raft length is varied, and on the vertical axis, the raft displacement is varied. The initial raft shape is shown in dark gray solid lines. The colored images show the deformed equilibrium shape, with the color indicating the displacement from the original position. The lighter the color, the more the raft is deformed. Flow is from left to right; streamlines are shown in light gray. Yellow crosses indicate the anchorage point.

around the raft. We were surprised to see that the raft edge is characterized by repeated fluctuations, associated with sequences of positive then negative magnitudes of $r(\theta, t)$ and vice versa. Consequently, the sign of $r(\theta, t)$ gave little useful information. These fluctuations defy a simple picture of ants leaving the edge due to a single measurement of critical stress: indeed, the raft is in a quasi-steady state where ants experience thousands of interactions with the edge over a 10 h time span. We decided against performing smoothing or interpretation of these fluctuations, which would require careful statistics. For simplicity, we opted to report the activity level as an absolute value.

In contrast with the exploration activity, the contraction of the raft is unaffected by the water flow. We used optical flow estimation to track the slow contraction of the raft, as detailed in the method section. Figure 4 shows the contraction velocity field throughout the trial for rafts in still water and in flow. The contraction rate is defined as the inward velocity towards the anchor and varies with location and time (red arrows in figure 4). In the graphs in figure 4, we plot the contraction rate (cm h^{-1}) as a function of radial position on the raft. This radial position is measured from the anchor. For all time periods, the contraction rate is on the scale of 1 cm h^{-1} and decreases with time. At early times (0–2.5 h), the contraction rate increases linearly with the distance from the anchor in both still and moving water. It is striking that the contraction rates of rafts in still water and in flow appear similar. This suggests that the contraction is simply due to the time elapsed rather than the influence of the flow. In later times, the magnitude of the contraction rate decreases, but the trend remains similar. In the next section, we present simulations with elastic rafts to give insight into our experimental results.

3.3. Fluid-structure interaction simulations

To understand the mechanical origin of the shape change, we perform a series of simulations using computational fluid dynamics and agent-based modeling. Note that these simulations only offer an approximate model for the raft. The biological ant raft is three-dimensional, rough on the scale of mm, and may have a slip layer because of its hydrophobicity. The three-dimensional drag would depend on the underwater profile called the draft. A complete picture of the system would have to include not only pressure drag and skin friction, but also wave drag. The anchor can also alter the flow profile and generate an unsteady von Kármán vortex street. Moreover, in nature, these forces would likely be amplified by any perturbations in the water and other currents. For the raft to remain anchored, it would have to resist all these forces. Given these differences, our goals here are to answer phenomenological questions and to estimate drag coefficients associated with the aspect ratios observed.

We observed shape change of the raft in our experiments, but how much of this shape change is due to passive deformation as opposed to active rearrangement of the ants? To answer this question, we perform simulations of flow past a purely elastic

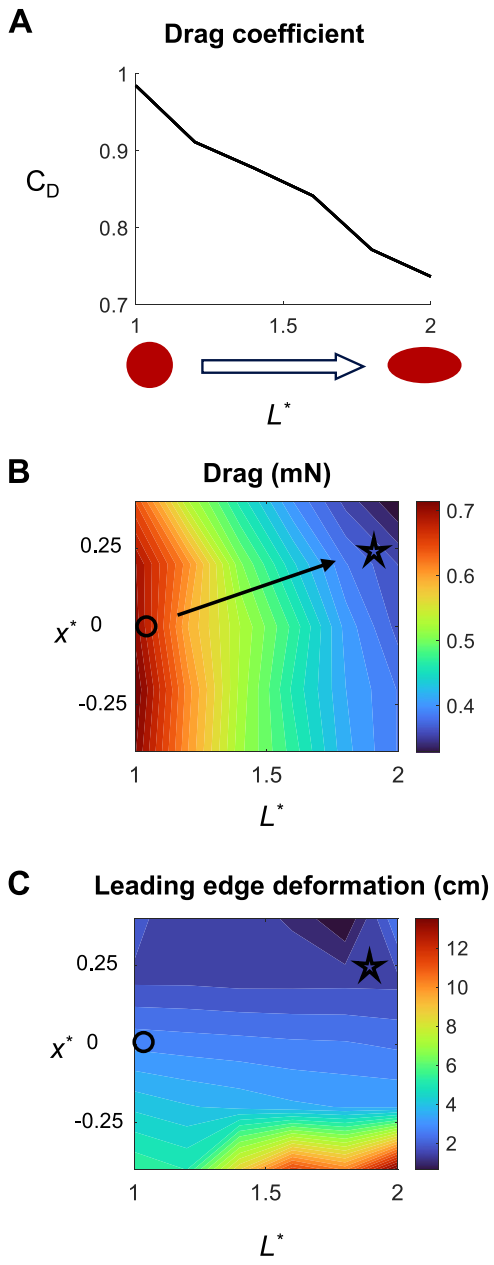

Figure 7. Elongation of fire ant rafts yield hydrodynamic benefits. (A) Simulated drag coefficient C_D as a function of the raft dimensionless length L^*. Phase diagram of (B) fluid drag and (C) the deformation of the leading edge as functions of dimensionless raft length L^* and dimensionless displacement x^*. The initial and streamlined configuration of the fire ant rafts from the experiment are marked by circles and stars, respectively.

ant raft of roughly the same size as that of our experiments as shown in figure 5. In our experiments, deformation occurred over several hours, yielding a shear rate on the order of 10^{-3} s^{-1}. We assume the Young's modulus of the raft is 200 Pa, which is associated with the shear rates of 1 s^{-1}, the closest data available to our desired regime [22].

Figure 5 displays an oblique and top view of the raft. The color indicates the magnitude of the water speed, with red colors associated with the highest speed and blue colors associated with the lowest speed. The inlet velocity matches that of the experiments, 0.6 cm s^{-1}. Since the presence of the raft reduces the channel width slightly, fluid accelerates to 0.8 m s^{-1} as it passes around the raft. Given the high Reynolds number of the flow, inertia dominates over viscous force and is the dominant force that deforms the raft. In our simulations, viscous force only makes up approximately 8.8% of the total drag.

We may use Bernoulli's theorem to relate the fluid velocities to the fluid pressure around the raft. The pressure is the highest at the stagnation point at the leading edge. At the trailing edge of the raft, the pressure is low due to secondary flows in the wake. As the flow accelerates past the flanks, the pressure is also low. If the anchor remains a fixed point on the raft, the fluid pressures should cause the elastic raft to compress at the leading edge, and stretch along the raft's flanks and trailing edge.

Figure 6 shows the deformation of the raft for various initial values of its dimensionless length L^* and dimensionless displacement x^*. Water flow is from left to right, with the solid black lines indicating the flow streamlines. The dark gray line encircling the raft indicates its original undeformed shape. The colors indicate the displacement field, with yellow having the greatest displacement and red having the least. In all conditions shown in figure 6, the deformation is most at the leading edge of the raft, shown by the yellow. The side and trailing edge of the raft are minimally stretched in all conditions, often only by less than 1 mm, as shown by the red colors there. This is in stark contrast with our experiments, in which rafts elongate greatly (around 10 mm) downstream.

Given that the elastic raft does not elongate in flow, we conclude that the elongation observed from our experiments is the result of complex social interactions that we will consider through using agent-based modeling in the next section. In our experiments, rafts exhibit high dimensionless length $L^* = 2$ and high displacement $x^* = 0.25$, similar to the initial condition shown in the top right graph of figure 6. This elongated configuration induces less deformation compared to our smulations of shorter rafts with lower displacement. Do elongated rafts reduce fluid drag as well?

Figure 7(A) shows the relation between drag coefficient C_D and the dimensionless length. Using the experimentally observed raft dimensionless lengths, the drag coefficient C_D reduces from 0.98 for a circle to 0.73 for the ellipse, a reduction of 26 percent. This trend is also shown in figure 7(B), which shows a heat map of the fluid drag force with changing raft length L^* and raft displacement x^*. The lowest drag is associated with a large raft length and large displacement. Fire ant rafts in the experiment started with dimensionless length $L^* = 1$ and dimensionless displacement $x^* = 0$, marked with a circle in the graph. Around 2 to 4 h after the trial, the elongated rafts had $L^* = 2$ and $x^* = 0.25$, marked with the

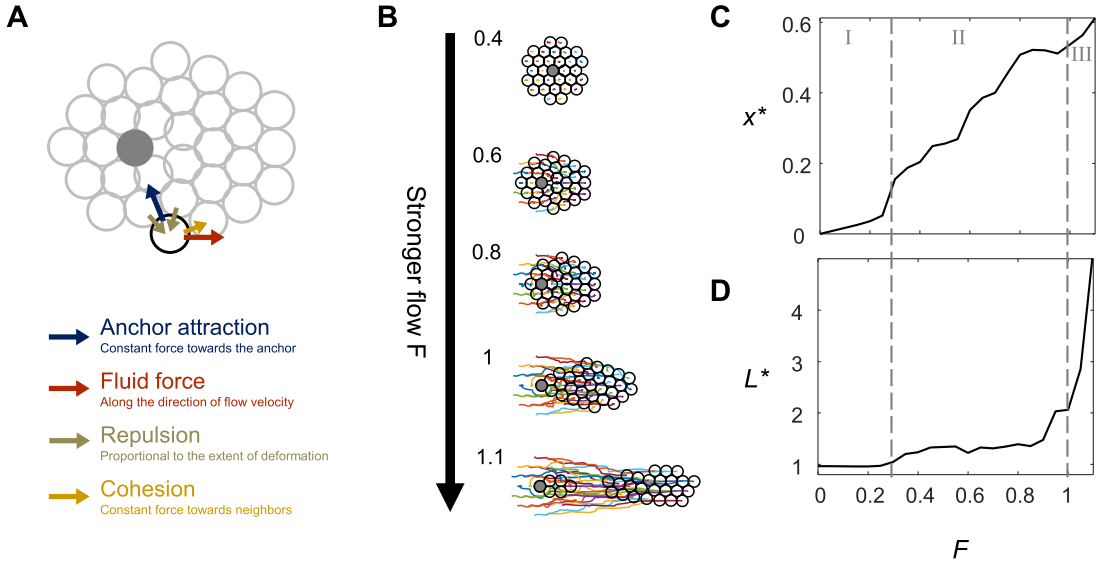

Figure 8. Agent-based simulations of ant raft deformation under different flow intensities. (A) Agents in the raft experience attraction to the anchor, fluid force, neighbor–neighbor repulsion to prevent overlap, and cohesion to neighbors to maintain contact. The gray circle represents the anchor, whose centroid is at least two radii away from the centroid of nearby agents. (B) Raft shapes as a function of F, the ratio of fluid force to attraction towards the anchor. (C) The relationship between L^* and dimensionless driving force (D) The relationship between x^* and dimensionless driving force. As F varies, the deformation goes from regime (I) elastic deformation, to (II) elongation, and (III) detachment.

star in the graph. Elongation reduces the fluid force by approximately 48%, from 0.71 mN to 0.37 mN. After reaching their optimal configuration, rafts start to shrink and decrease in both x^* and L^* (see figure 2). Shrinking causes the rafts to be more circular and thus less streamlined. However, the drag force remains low due to the reduced cross-sectional area.

Figure 7(C) shows a heat map of the leading edge displacement with changing raft length L^* and displacement x^*. It shows that the leading edge compression is more affected by displacement than raft length. Rafts with larger displacement x^* of their center of mass deform less at the leading edge, which we have also demonstrated in figure 6. In summary, we find that by displacing and stretching, rafts can reduce their leading edge compression and their drag. The reduced mechanical load may prevent breakage, increase stability, and reduce the metabolic demand of the ants.

3.4. Agent-based simulations

Because the ant raft is so fragile, it is challenging to experimentally measure the change in raft shape with faster flow. Instead, we approach this problem with agent-based simulations. As discussed in the methods section, each ant experiences five forces, including a fluid force, attraction to the anchor, attraction to their neighbors, damping, and repulsion from their neighbors to avoid overlap.

Due to the difficulty simulating the fluid field as the raft deforms, we assume a static flow field. Specifically, the fluid flow field is generated by interaction between a constant uniform flow and the cylindrical anchor. The flow streamlines are given by thepotential flow solution around a cylinder. The ants do not influence the flow. Instead, the fluid force on an ant is proportional to the local flow velocity vector. In addition, each ant experiences an attractive force towards the anchor. This force may be considered a 'social force' that mimics an ant's knowledge of the anchor location and its desire to move towards it. Similar forces have been applied in most flocking models, such as the classical Boids model [30]. Without the anchor attraction, and under inter-particle adhesion alone, rafts behave like water droplets with a high surface tension and remain circular even when the flow is strong enough to dislodge them. This physical picture is clearly very different from the elongation observed in experiments. We proceed by refuting our hypothesis that ants have only local sensing. In this simulation, we assume that ants acquire global information about the state of the raft and the anchor over a span of hours. The ratio between the fluid force and the anchor attraction, F, represents the relative intensity of the flow.

Figure 8(A) shows that as the flow becomes stronger, the raft lengthens and displaces. Figures 8(B) and (C) reveals three regimes of deformation, labelled I, II, and III in the graphs. At low flow intensities $F < 0.2$, rafts deform elastically. In this regime, agents maintain their relative positions, displacing only slightly. At intermediate flow intensities $0.2 < F < 1$, agents rearrange in response to flow, as shown by the change in overall raft shape and the increase in both raft displacement x^* and raft length L^* as observed in experiments. As flow intensity passes a threshold $F > 1$, the raft increases in length and

can no longer maintain its grip on the anchor. Separation ensues. The fragility of rafts at high speed is consistent with experimental trials at flow speeds of 15 cm s^{-1}. As the fluid stress exceeds a certain threshold, the raft may break into smaller satellite rafts. This observation is reminiscent of hard coral *Acropora cervicornis*. Instead of deforming, they break into fragments which quickly re-anchor and re-grow rapidly [31].

These regimes seem physically reasonable, but future experiments are required to verify the thresholds and the trends in displacement and length. It would also be of interest to study how the transition is affected by the size of the rafts.

3.5. Discussion

In this study, we showed that rafts streamline by shrinking laterally and elongating downstream. Moreover, they can displace themselves relative to their anchorage point, which reduces the deformation at the leading edge of the raft. To obtain information on the shape and flow around the raft,ants explored the edge of the raft. We performed measurements of ant activity at the boundary, finding that initially, activity is homogeneous at all positions on the boundary. As time goes on, the activity becomes heterogeneous with less activity at the leading edge.

One hypothesis for this behavior is that free-roaming ants settle at boundary locations of lower fluid stress. This would be reminiscent of previous models of a flock of penguins huddling in a cold wind [32]. The penguin that experiences the highest heat loss rate would change location; penguins in the middle overheat, so they too must go towards the boundary. The varying heat transfer with position drives the perpetual flow of penguins. In this study, we also observed activity levels varying with position on the boundary and distance from the anchor. Further work is needed to determine if ants learn about the flow from sensing at the edge.

We presented an agent-based model that indicated that elongation of the raft is only possible if the ants have global information, specifically, their distance and direction from the anchorage point. Our work showed comparable behavior to experiments, but further work is required. The number of agents we used is low compared to the number of ants on the raft. Moreover, in our simulations, agents have identical sizes (monodisperse) and can only move in two dimensions. These factors may have prevented our simulated rafts from deforming to the extent of biological ant rafts. Future studies will need to iteratively simulate the fluid field while updating agent locations in each time step. This is because of the interaction of the shape of the raft and the fluid stress . Due to the high computational cost, fluid-agent interaction simulations are rare in the literature (see [33] for an example).

Our fluid-structure interaction simulations captured the passive deformation of the raft, but the nature of the active deformation raises further questions for future study. What is the ants' response function, and how does it depend on the time scale of the force? These questions are intrinsically about the properties of ant rafts as materials, which can be obtained through subjecting them to perturbation of a range of magnitudes and time scales. Rheological work on ants [22] noted that ant aggregations lack a signature relaxation timescale. As non-equilibrium materials, it may be challenging to categorize living aggregations into any canonical viscoelastic models.

The line between the active response of the material and clever mechanical design is unclear. The mechanical designs of grass and shrubs allow them to adopt different drag reduction strategies: the former decreases cross-flow area, and the latter becomes more porous [15]. These responses do not require any activity; they simply take advantage of clever mechanical design that evolved over years of natural selection. Liquid droplets also deform under external flows in ways that may reduce drag [34–37]. The fluid-like behavior we observed may only require activity, but not any planning or communication among the group. We found black soldier fly larvae do not require any sensing of their environment to reduce flow hysteresis; they only require random body motions, which generate rearrangement of the collective [33]. Could the streamlining behavior be a consequence of just random motion, or does it truly require sensing?

In previous work, we rationalized the initial rapid expansion of the raft based on the liquid–solid behavior of the material. Specifically, initially, the raft is many layers, and gravitational forces cause the ants to break their connections and flow outward. Once the raft reaches two layers, the stress is sufficiently low for the ants to act more solid-like. Such flow at high stresses and elastic behavior at low stresses was shown through the shear rheology of the ants. The slow contraction of the ants over 10 h is a robust result that occurs both in still water and in flow. Isometric contraction does not require information about the global state. We speculate that contraction may occur as the ants run out of resources, similar to how slime molds *Dictyostelium* contract before forming fruiting bodies [38, 39].

An important next step for future workers is direct drag force measurement of the ant raft, which would enable direct comparisons of the simulations and the experiment. We predicted the drag forces to be approximately 0.7 mN. A force sensor that could measure this magnitude of drag force would need to be compact, waterproof, and flexible enough to be placed on the surface of the rod. Any setup that measures the total drag on the anchor would need to subtract the contribution from the anchor itself. In the past, workers used elastic bands to measure the

force between two ants ([1]). An elastic band on the water surface would flutter due to the incoming flow. Devices that extend into the water from the air would also suffer from ants crawling on them. Conducting 10 h long measurements for forces on the scale of millinewtons on the water with actively crawling ants is indeed a challenging task that remains unsolved.

4. Conclusion

Animal swarms must stick together in the face of flowing water and wind. Despite the ubiquity of such flows in nature, most studies of swarms assume static conditions. In this study, we show how an ant raft responds while it is pulled by the surrounding flow. We show in experiments that the fire ant raft displaces from the anchor and stretches downstream. This shape change is accompanied by changes in exploration behavior: ants explore the leading edge of the raft less than the flanks and trailing edges. The edge of the raft is characterized by fluctuations in the short run. In the long run, ants migrate from the leading edge to points downstream.

In parallel with our experiments, we performed 'knock-out experiments' with numerical simulations by modifying the ants' material properties. We model the fluid flow past a purely elastic raft with the same elasticity of ants as found by rheological experiments. Simulations of a smooth raft of comparable dimensions suggest that the stretching of the ant rafts may reduce drag up to 48% compared to its original unperturbed shape. Moreover, we discover that an elastic raft does not elongate in flow; conversely, it flattens its leading edge and in fact, widens in response to flow. This contrast with experiments indicates that raft elongation is an active response from the ants. Agent-based simulations show elongation similarto the biological ant raft and breakage when fluid forces are sufficiently high. A cohesive force between agents was insufficient to hold the rafts together. For the raft to elongate, simulated ants require an attractive force towards the anchor, suggesting that in the experiments, ants have obtained global information about the raft over a span of hours and thousands of interactions. Our work with simplified models is a first step towards understanding the sophisticated behavior we observe in our experiments. We hope that further work in this area will provide insights into designing robot swarms that can adapt to fluid disturbances in the wild.

Acknowledgments

This work is funded by Army Research Office-Grant W911NF-19-1-0086.

Data availability statement

All data that support the findings of this study are included within the article (and any supplementary files).

ORCID iDs

Hungtang Ko https://orcid.org/0000-0001-6250-6144
David L Hu https://orcid.org/0000-0002-0017-7303

References

[1] Mlot N J, Tovey C A and Hu D L 2011 Fire ants self-assemble into waterproof rafts to survive floods *Proc. Natl Acad. Sci. USA* **108** 7669–73
[2] Adams B J, Hooper-Bùi L M, Strecker R M and O'Brien D M 2011 Raft formation by the red imported fire ant, *Solenopsis invicta J. Insect Sci.* **11** 171
[3] Mlot N J, Tovey C and Hu D L 2012 Dynamics and shape of large fire ant rafts *Commun. Integr. Biol.* **5** 590–7
[4] Wagner R J, Such K, Hobbs E and Verneret F J 2021 Treadmilling and dynamic protrusions in fire ant rafts *J. R. Soc. Interface* **18** 20210213
[5] Harder D L, Speck O, Hurd C L and Speck T 2004 Reconfiguration as a prerequisite for survival in highly unstable flow-dominated habitats *J. Plant Growth Regul.* **23** 98–107
[6] Koehl M A R 1984 How do benthic organisms withstand moving water? *Am. Zool.* **24** 57–70
[7] Koehl M A R 1982 The interaction of moving water and sessile organisms *Sci. Am.* **247** 124–34
[8] Vogel S 1984 Drag and flexibility in sessile organisms *Am. Zool.* **24** 37–44
[9] Gaylord B, Blanchette C A and Denny M W 1994 Mechanical consequences of size in wave-swept algae *Ecol. Monogr.* **64** 287–313
[10] Graus R R, Chamberlain J A Jr and Boker A M 1977 Structural modification of corals in relation to waves and currents: reef biota *Reefs and Related Carbonates—Ecology and Sedimentology* (Tulsa: American Association of Petroleum Geologists)
[11] Chang-Feng D and Ming-Chao L 1993 The effects of flow on feeding of three gorgonians from southern Taiwan *J. Exp. Mar. Biol. Ecol.* **173** 57–69
[12] Sponaugle S and LaBarbera M 1991 Drag-induced deformation: a functional feeding strategy in two species of gorgonians *J. Exp. Mar. Biol. Ecol.* **148** 121–34
[13] De Langre E 2008 Effects of wind on plants *Annu. Rev. Fluid Mech.* **40** 141–68
[14] Cleugh H A, Miller J M and Böhm M 1998 Direct mechanical effects of wind on crops *Agrofor. Syst.* **41** 85–112
[15] Gardiner B, Berry P and Moulia B 2016 Review: wind impacts on plant growth, mechanics and damage *Plant Sci.* **245** 94–118
[16] Vogel S 1989 Drag and reconfiguration of broad leaves in high winds *J. Exp. Bot.* **40** 941–8
[17] Vollsinger S, Mitchell S J, Byrne K E, Novak M D and Rudnicki M 2005 Wind tunnel measurements of crown streamlining and drag relationships for several hardwood species *Can. J. For. Res.* **35** 1238–49
[18] Mayhead G J 1973 Some drag coefficients for British forest trees derived from wind tunnel studies *Agric. Meteorol.* **12** 123–30

[19] Rudnicki M, Mitchell S J and Novak M D 2004 Wind tunnel measurements of crown streamlining and drag relationships for three conifer species *Can. J. For. Res.* **34** 666–76
[20] Pinthus M J 1974 Lodging in wheat, barley, and oats: the phenomenon, its causes, and preventive measures *Adv. Agron.* **25** 209–63
[21] Telewski F W 2012 Is windswept tree growth negative thigmotropism? *Plant Sci.* **184** 20–8
[22] Tennenbaum M, Liu Z, Hu D and Fernandez-Nieves A 2016 Mechanics of fire ant aggregations *Nat. Mater.* **15** 54–9
[23] Shishkov O, Trebuchon J, Yunker P J, Franklin S and Hu D L 2019 Black soldier fly larvae rearrange under compression *Integr. Comp. Biol.* **59** 1646–52
[24] van der Vaart K, Sinhuber M, Reynolds A M and Ouellette N T 2019 Mechanical spectroscopy of insect swarms *Sci. Adv.* **5** eaaw9305
[25] Peleg O, Peters J M, Salcedo M K and Mahadevan L 2018 Collective mechanical adaptation of honeybee swarms *Nat. Phys.* **14** 1193–8
[26] Horn B K P and Schunck B G 1981 Determining optical flow *Artif. Intell.* **17** 185–203
[27] Batchelor C K and Batchelor G 2000 *An Introduction to Fluid Dynamics* (Cambridge: Cambridge University Press)
[28] Schweitzer S A and Cowen E A 2021 Instantaneous river-wide water surface velocity field measurements at centimeter scales using infrared quantitative image velocimetry *Water Resour. Res.* **57** e2020WR029279
[29] Stern D A, Khanbilvardi R, Alair J C and Richardson W 2001 Description of flow through a natural wetland using dye tracer tests *Ecol. Eng.* **18** 173–84
[30] Reynolds C W 1987 Flocks, herds and schools: a distributed behavioral model *Proc. 14th Annual Conf. Computer Graphics and Interactive Techniques* pp 25–34
[31] Tunnicliffe V 1981 Breakage and propagation of the stony coral *Acropora cervicornis Proc. Natl Acad. Sci. USA* **78** 2427–31
[32] Waters A, Blanchette F and Kim A D 2012 Modeling huddling penguins *PLoS One* **7** e50277
[33] Ko H, Cassidy G J, Shishkov O, Aydin E, Hu D L and Goldman D I 2021 Air-fluidized aggregates of black soldier fly larvae *Front. Phys.* **9** 663
[34] Dimitrakopoulos P and Higdon J J L 1997 Displacement of fluid droplets from solid surfaces in low-Reynolds-number shear flows *J. Fluid Mech.* **336** 351–78
[35] Feng J Q and Basaran O A 1994 Shear flow over a translationally symmetric cylindrical bubble pinned on a slot in a plane wall *J. Fluid Mech.* **275** 351–78
[36] Shirani E and Masoomi S 2008 Deformation of a droplet in a channel flow *J. Fuel Cell Sci. Technol.* **5** 041008
[37] Seevaratnam G K, Ding H, Michel O, Heng J Y Y and Matar O K 2010 Laminar flow deformation of a droplet adhering to a wall in a channel *Chem. Eng. Sci.* **65** 4523–34
[38] Raper K B 1940 Pseudoplasmodium formation and organization in *Dictyostelium discoideum J. Elisha Mitchell Sci. Soc.* **56** 241–82
[39] Loomis W 2012 *The Development of Dictyostelium Discoideum* (Amsterdam: Elsevier)